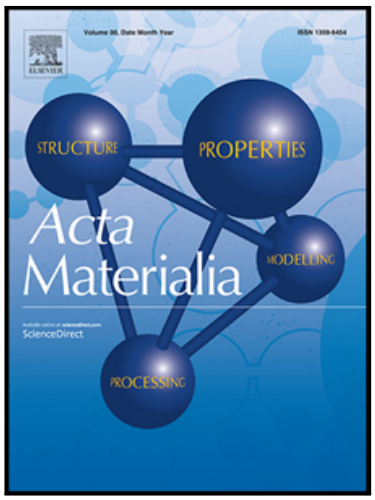

Direct observation of the dynamic evolution of precipitates in aluminium alloy 7021 at high strain rates via high energy synchrotron X-rays

W.U. Mirihanage , J.D. Robson , S. Mishra , P. Hidalgo-Manrique , J. Quinta da Fonseca , C.S. Daniel , P.B. Prangnell , S. Michalik , O.V. Magdysyuk , T. Connolley , M. Drakopoulos

PII: S1359-6454(20)30969-1
DOI: https://doi.org/10.1016/j.actamat.2020.116532
Reference: AM 116532

To appear in: *Acta Materialia*

Received date: 16 March 2020
Revised date: 28 November 2020
Accepted date: 28 November 2020

Please cite this article as: W.U. Mirihanage , J.D. Robson , S. Mishra , P. Hidalgo-Manrique , J. Quinta da Fonseca , C.S. Daniel , P.B. Prangnell , S. Michalik , O.V. Magdysyuk , T. Connolley , M. Drakopoulos , Direct observation of the dynamic evolution of precipitates in aluminium alloy 7021 at high strain rates via high energy synchrotron X-rays, *Acta Materialia* (2020), doi: https://doi.org/10.1016/j.actamat.2020.116532

Direct observation of the dynamic evolution of precipitates in aluminium alloy 7021 at high strain rates via high energy synchrotron X-rays

W.U. Mirihanage[1,*], J. D. Robson[1], S. Mishra[1], P. Hidalgo-Manrique[1], J. Quinta da Fonseca[1], C. S. Daniel[1], P. B. Prangnell, S. Michalik[2], O. V. Magdysyuk[2], T. Connolley[2], M. Drakopoulos[2]

[1]Department of Materials, University of Manchester, Manchester M13 9PL, UK

[2]Diamond Light Source, Didcot OX11 0DE, UK

*Corresponding author email: wajira.mirihanage@manchester.ac.uk

Abstract

An improved understanding of the phenomenon of dynamic precipitation is important to accurately model and simulate many industrial manufacturing processes with high strength Al-alloys. Dynamic ageing in 7xxx Al-alloys can occur as a result of both the strain and heat. Small angle X-ray scattering (SAXS) is an advanced technique that allows the precipitation processes to be studied in situ, but to date this has only been possible at lower than industrially relevant strain rates (e.g. $< 10^{-3}$). In this contribution, we demonstrate the potential of in-situ SAXS studies of metallic alloys at higher strain rates (10^{-2}) than previously, using a high energy synchrotron X-ray. The time resolved SAXS information has been used to evaluate dynamic precipitate evolution models and has demonstrated that at high strain rates a new regime must be considered which includes the more significant effect of vacancy annihilation, leading to a clear strain rate, rather than just strain, kinetic dependence.

1. Introduction

High strength 7xxx aluminium alloys obtain their properties through the formation of precipitates. The required precipitate distribution is usually obtained through controlled heat treatment performed in the absence of an applied strain. However, there are scenarios where precipitation can occur concomitantly with deformation. One example is during in warm forming (for example, in the range 423-523 K). This is an attractive option for producing shaped parts from high strength aluminium sheet and some recent examples of this approach for 7xxx aluminium alloys are given in [1-4].

Temperatures in this range are below the solvus temperature for the precipitate phases and thus precipitation will evolve under the action of both heat and deformation [5]. In the case of commercial warm forming, the initial state prior to warm forming is anticipated to be partially supersaturated in solute following a stabilization pre-temper, and thus deformation can influence the further decomposition of the solid solution during the forming operation.

It has been widely shown that under such conditions, deformation leads to very strong changes in the kinetics of precipitate evolution when compared with heating alone [6-8] In particular, strong ódynamic agingô effects have been observed in Al-Zn-Mg alloys at moderate temperatures [7], at room temperature [6], and even down to cryogenic temperatures [9]. Given its practical and theoretical importance, the topic of plasticity assisted precipitate evolution has received considerable attention [8]. This field of research has recently been reinvigorated by the advent of experimental tools that enable the complex interactions between plasticity and precipitation to be studied in-situ during deformation [6, 7, 10].

Deschamps and co-workers [6, 7, 9-11] have pioneered the development of small angle X-ray scattering (SAXS) to study the dynamic interaction of deformation and precipitation in Al-Zn-Mg-(Cu) (7xxx) alloys and identify the mechanisms of interaction. It has been demonstrated that dynamic interaction between dislocations and precipitates is complicated and depends on various intrinsic and extrinsic factors, such as the degree of supersaturation, temperature, strain and strain rate.

Regardless of the initial state (e.g. a supersaturated solid solution or pre-aged to a maximum precipitate volume fraction (T6) temper) it has been consistently shown that plasticity strongly accelerates the kinetic processes that govern precipitate evolution. The strongest dynamic effects are observed when the initial solution supersaturation is greatest [7]. This is to be expected, since in the as-quenched supersaturated state, when there is a high driving force, plasticity has an accelerating effect on both the precipitate nucleation and growth processes. In the case where precipitation is complete, deformation can still have a profound effect on the evolution of the precipitate population, but this occurs mainly through accelerated precipitate coarsening [7, 11]. Other phenomena that can also occur in an underaged state, where precipitates are small enough to be cut by dislocations, include partial or complete dissolution by particle shearing [12, 13] or generation of bi-modal precipitate populations due to new plasticity induced precipitate nucleation [10].

Two additional important observations have emerged from in-situ studies of dynamic precipitation in Al-Zn-Mg-Cu alloys [7]. The first is that direct precipitation on dislocations is not sufficient to explain the accelerating effect of plasticity. Indeed, the dynamically formed precipitates are often remarkably uniform in both distribution and size [5, 10]. The second observation is that the accelerating effect of plasticity on precipitation kinetics is linearly dependent on strain but is either insensitive to strain rate or shows a negative strain rate sensitivity (at a given strain value [7, 10]). These observations have been rationalized on the basis that deformation induced vacancies [14] are the primary factor leading to the accelerating effect of plasticity.

The results of in-situ studies reported to date have been confined to relatively low strain rates. For example, the maximum rate studied by Deschamps et al. was 4 x 10^{-4} s^{-1} [7], and the maximum achieved in other in-situ studies does not exceed 2 x 10^{-3} s^{-1}. Studies at higher strain rate have also been performed, but only using ex-situ analysis, making interpretation of the results more difficult [11]. Nevertheless, there is some evidence that towards the higher strain rates studied by both in-situ and ex-situ methods, the insensitivity of precipitate growth rate to strain rate observed in [7] (at lower strain rates) may not hold [10, 11].

The capacity of SAXS to characterize sub-micron range precipitates in metallic alloys has been successfully demonstrated in previous studies [15, 16]. The recorded scattering intensity derives from the beam interaction difference between the precipitate phase(s) and the matrix along with the inter-particle correlations. If these correlations are isotropic, then the total scattering intensity) Ñ can be represented as (q = 4´ Sinɗ/ɤ; 2ɗ is the scattering angle and ɤ is the wavelength)

ρ

where I_0 is the intensity of the incident beam, $6_{ę}$ is the volume of the precipitates, $ɟ_p$ and $ɟ_m$ are the scattering length density for precipitates and matrix, respectively. S(q) represents a structure factor term, describing the arrangement of precipitates of a given form factor F(q), within the illuminated sample volume and B is a background related constant.

A number of in-situ SAXS studies that used synchrotron radiation or lab sources (often with Cu K_α) to study dynamic precipitation process have been reported previously e.g. [7, 10, 15, 16]. However, these in-situ experiments are usually conducted at dedicated

synchrotron SAXS beamlines. Typically, most dedicated SAXS synchrotron beamlines operate with photon energies below 20 keV with moderate photon flux densities. These experimental conditions limit the thickness of metallic samples (even for aluminium) to a maximum of around 0.5mm, thus producing a signal from a small sample volume. It becomes challenging to control the deformation of such thin specimens to obtain stable deformation as strain rate increases. Defects and inclusions that are typical of industrially produced aluminium alloys can lead to early failure of such thin specimens through strain localization since a single large constituent particle may occupy a significant portion of the sample thickness.

The primary purpose of the present work was to use high energy X-rays to perform in-situ experiments at a higher strain rate with thicker specimens than previously reported, more closely approaching the conditions used in actual forming operations. A thicker specimen, as enabled by the use of higher energy X-rays (>50 keV) in the present study, provides better opportunities to control the deformation behaviour, strain rate and higher level of strain before strain localization associated failure.

2. Experimental

The commercial aluminium alloy AA7021, supplied by Constellium C-TEC with composition Al-5.8Zn-1.4Mg-0.19Cu-0.2Fe-0.057Mn-0.058Si (wt%), was used for performing the experiments. The as received 2 mm gauge sheets of AA 7021 were supplied in a T4P temper condition and were machined in to 20 mm gauge length 1 mm x 2 mm rectangular cross section ômatch-stickô samples. The sheet is commercially rolled from a direct-chill cast ingot that is first homogenized. After rolling, solution treatment is applied commercially and the stabilization (pre-aging) temper (T4P) was performed. As will be demonstrated later, this establishes a pre-existing precipitate population, which evolves during the experiment.

To perform in-situ dynamic straining experiments at controlled temperatures, an Instron-8800 electro-thermal mechanical testing (ETMT) system was integrated into the beamline. The T4P samples were heated to 463 K at a rate of 0.85 K s^{-1}, followed by a hold period of 300 s. The samples were then deformed in uniaxial tension at nominal strain rates of 10^{-3} s^{-1} and 10^{-2} s^{-1}. The total strain imposed on the samples was kept constant at 0.2.

The in-situ SAXS experiments were conducted at beamline I12, at the Diamond Light Source, UK. I12 beamline is a general engineering beamline with a wiggler that produces

very high energy X-rays. Moreover, the beamline layout allows the placement of detectors as far as 30 metres away from the sample stage. The SAXS experiments were conducted with 61.5 keV monochromatic X-rays. The ETMT samples were configured so that a 0.4 x 0.4 mm^2 X-ray beam passed through the centre of the sample in thickness direction and the transmitted scattered beam was collected on a flat panel Pixium RF4343 detector, placed 29.73 m away from the sample (with a vacuum between the sample and detector). The X-ray scattering signal was collected at a rate of 1 Hz with a 0.95 s exposure time. The raw data were recorded as image files and preliminary treated to remove the instrumental background. The integrated data was then corrected for absorption and scattering length. No absolute intensity calibration was made; hence intensity is given in arbitrary units. However, experimental conditions presented here are similar and comparable with each other. All the image processing was performed through bespoke Matlab® scripts. Unlike with traditional SAXS beamlines, due to the high photon energy the beamstop was not equipped with a diode for setting up the experiments. Therefore, calibration greyscale measurements were collected using a scintillator coupled camera (Pco.Edge) system and the full image field view of the camera (with opened slits) was used to adjust the sample placement.

For corroboration purposes, Transmission electron microscopy (TEM) of the processed samples was performed using a TALOS F200X TEM. Sample preparation was carried out via twin jet electropolishing with a mixture of 70% methanol and 30% nitric at 30 ^{o}C. For selected sample conditions, particle size distributions were obtained from multiple TEM images using ImageJ software. A low pass filter was first applied to adaptively remove the background. Subsequently, the particle size distributions were extracted through an ImageJ plugin.

3. Results

The initial state of the as received T4P sample was estimated via standard uniaxial tensile tests at room temperature. The tensile test results are shown in Fig.1. It can be observed that the yield (0.2% proof) strength of the T4P sample was 330 MPa, which is approximately 80% of the T6 strength (407 MPa [17]). Therefore, most of the initial (as-quenched) supersaturation has already been lost to precipitation during the extended natural aging/ stabilization treatment. As demonstrated later, the starting supersaturation for this material was therefore sufficiently low so that further precipitate evolution was dominated by growth and coarsening and not nucleation.

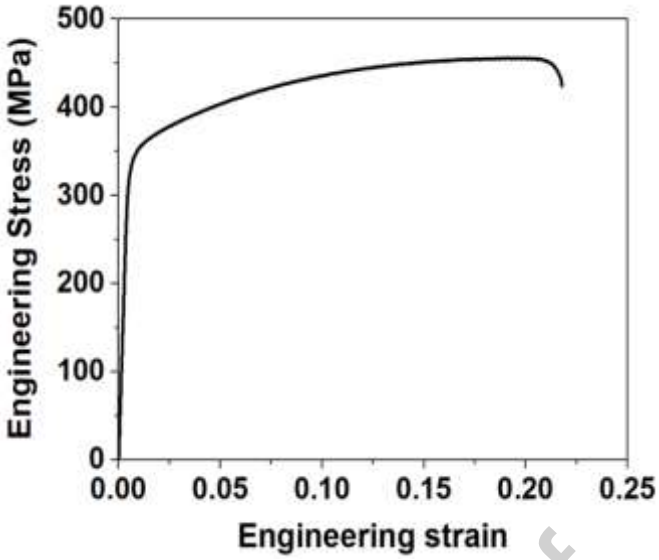

Fig. 1 Engineering stress versus strain curve of the as received T4 sample.

To enable quantitative analysis, the SAXS intensity data was converted into Kratky representation (Iq^2 versus q). Time evolution of the Kratky representation for both the strain rates are shown in Fig. 2.a-b, where it can be observed that the intensity in the lower q range increases substantially with time and that the total increase in intensity was greater for the slow strain (10^{-3}) rate tests compared to the high strain rate (10^{-2}) tests. For clarity, and to enable direct comparison on the basis of the strain, the I versus q plots are only presented every 10 readings for the slow strain rate sample, while SAXS data in terms of intensity (I) vs scattering vector (q) plots are shown in enclosed in Fig. 2 as coloured figures. In addition, it can also be observed that the scattering vector corresponding to intensity maxima in the Kratky plots (q_{max}), which is inversely proportional to the average size of the precipitates (R_g), decreases with time for both strain rates (insets in Fig. 2) [15, 16]. In both cases, the initial peak appears at q = 1.6 nm^{-1}, while at a strain of 0.2, after 200 s and 20 s of deformation respectively for the two different stain rates, the peaks have moved to approximately 1.2 ï 1.25 nm^{-1} although the peak profiles appear slightly different with the high-strain rate sample peaks displaced to slightly lower q values. This demonstrates that despite the order of magnitude difference in strain rate, and therefore time between the two experiments, the total change in average precipitate size is similar, but subtle differences have occurred.

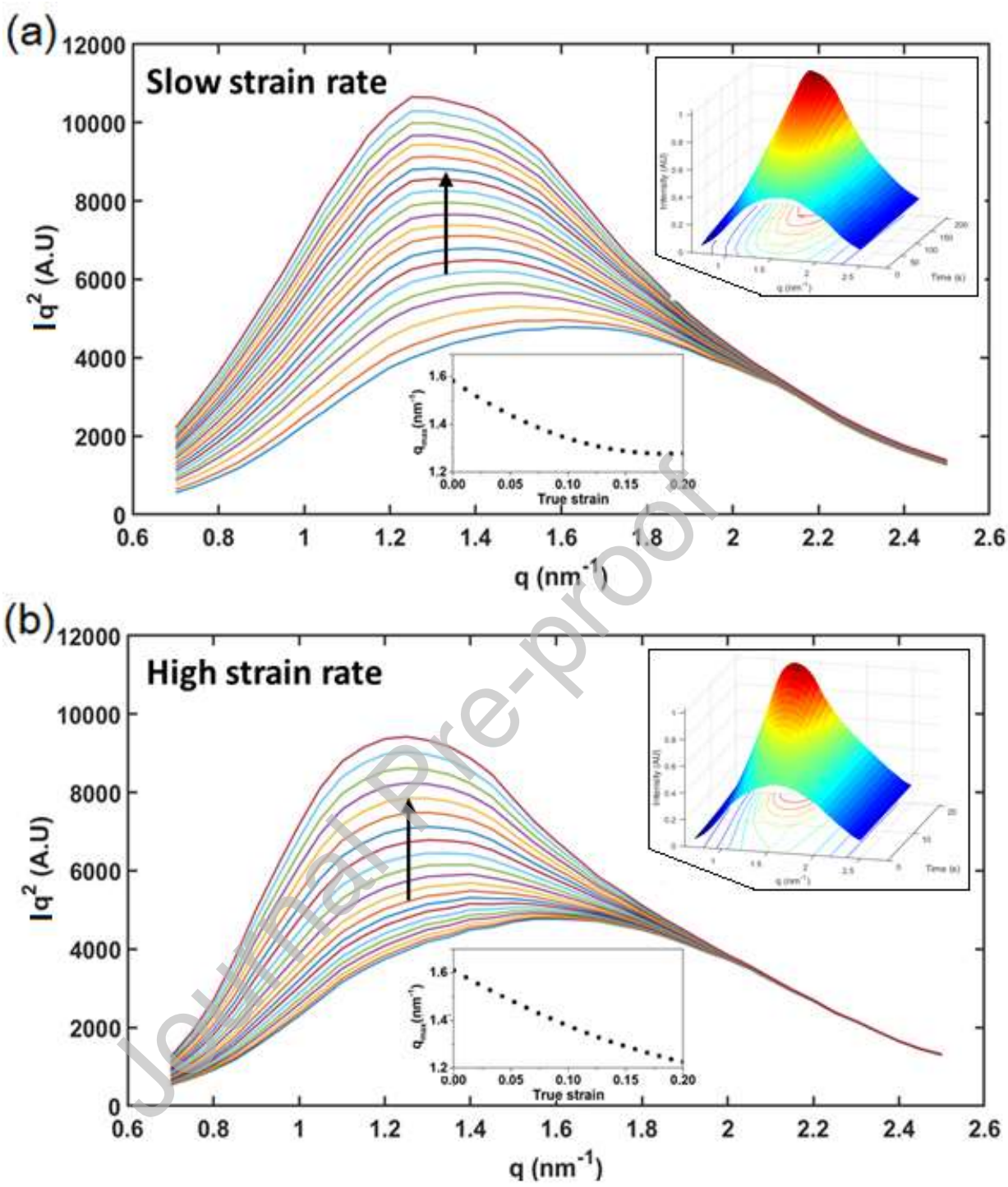

Fig. 2 Kratky plots for (a) the slow strain rate (10^{-3}) and (b) high strain rate (10^{-2}) sample. The arrow direction indicates the evolution of Kratky plots with time. The insets in each figure shows the evolution of the scattering vector corresponding to the intensity maxima with strain and evolution of intensity versus scattering vector plots (in colour).

To better illustrate the interplay between the test parameters and precipitate evolution in more detail, selected examples of direct comparisons between the Kratky plots are provided in Fig. 3, firstly at constant strain (Fig. 3.a-d) and then at constant time (Fig. 3.e-f). It can be observed that for starting condition (Fig. 3.a), the Kratky plots for each strain rate overlap, confirming that prior to deformation both specimens contain similar precipitate/GPZ distributions, as expected. However, with increase in plastic strain (Fig. 3.b-d), clear differences between the two strain rates develop. These differences are apparent, even at a small value of the applied strain (1%, Fig. 3.b). In both cases, as the strain (and hence also time) increases, the area under the Kratky plot increases and the peaks shift to smaller q values. This corresponds to an increase in average size. At a given level of strain, these changes are greatest for the slow strain rate case. This is not surprising, since for a given level of strain, the slow strain rate specimen will have been deformed for 10 times longer allowing more time for diffusion to take place It is also interesting to compare the high and low strain rate conditions for the same deformation time. In this case, the specimen deformed at high strain rate will experienced 10 times greater strain than that deformed at low strain rate. This comparison shows a strong effect of strain on the evolution of the precipitates; i.e. the high strain rate (and therefore high strain) condition leads to a much greater precipitate average size and an increase in volume fraction after 20s deformation, compared to the low strain rate (low strain) case. This strong accelerating effect of increasing strain on precipitate evolution is consistent with previous work [7, 10].

To quantitatively compare the precipitation states for the two deformation conditions, the evolution of the integrated intensity (area under the Kratky plot) and average domain radius with plastic strain and time is illustrated in Fig. 4. These graphs confirm the trends highlighted in Fig. 4, in that the strong accelerating effect of strain on the kinetics is apparent when the evolution of the integrated intensity is plotted as a function of time. However, this acceleration is insufficient to compensate for the reduced time at high strain rates; this is apparent when the data is plotted as a function of strain (recalling that for iso-strain, the low strain rate sample has experienced 10 times longer exposure than the high strain rate sample). Interestingly, when comparing the average radius evolution as a function of strain, the data from the low and high strain rate conditions are very close (and within the error of 0.5 nm as a result of data binning). This suggests that for the conditions studied here, the acceleration of the precipitate growth, or coarsening kinetics, due to the high strain rate almost exactly compensates for the 10 times reduction in time to reach the same strain.

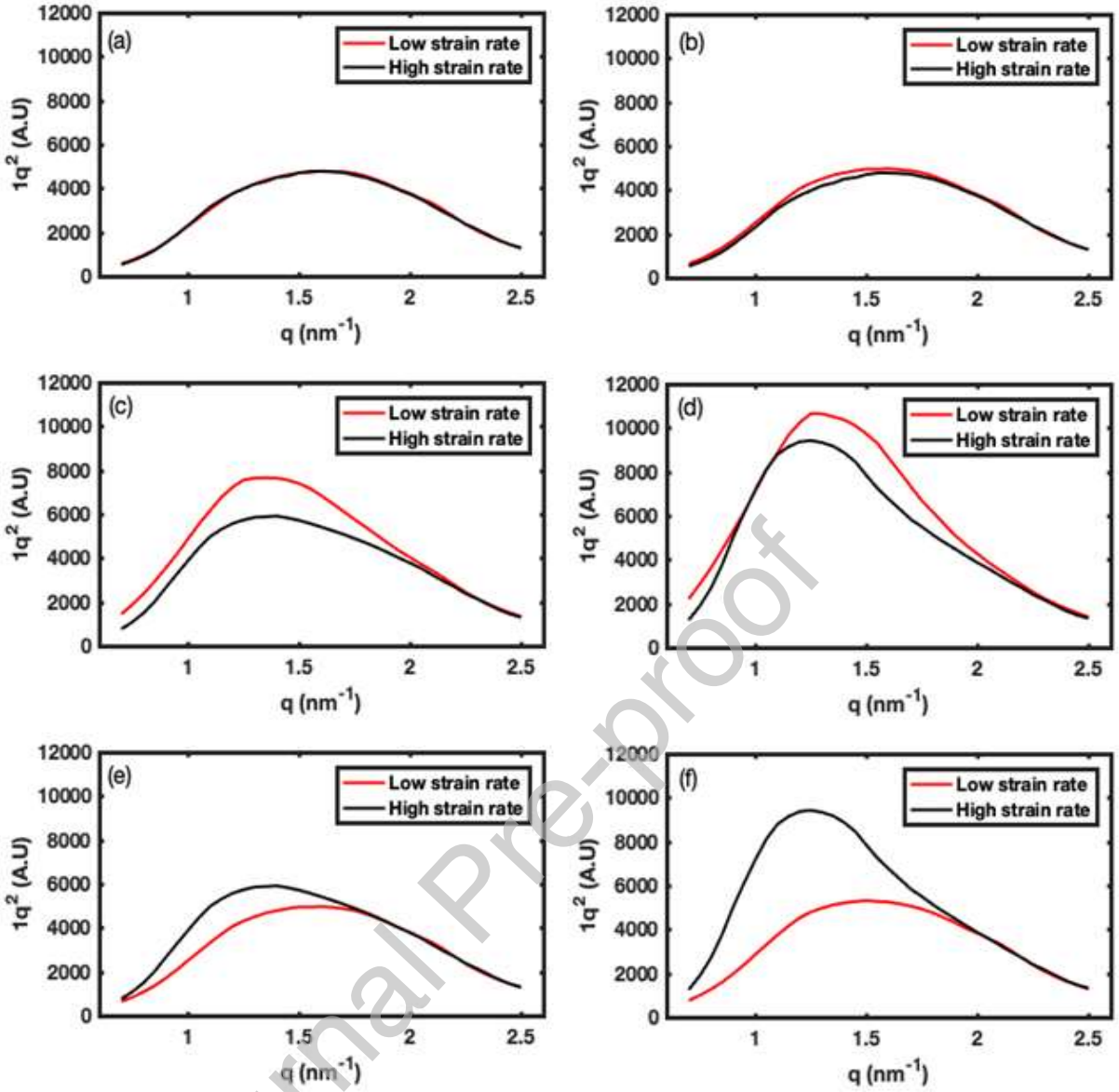

Fig. 3 Comparison of Kratky plots at different levels of strain (a) 0 (b) 0.01 (c) 0.1 (d) 0.2 and at different time intervals (e) 10 seconds (f) 20 seconds.

To determine whether the changes in integrated intensity and average radius were likely to be due to nucleation and growth of a new precipitate population, or the evolution of GPZs/precipitates inherited from the T4P condition and initial heating rate and 300 s hold step, an estimate was made of the number density evolution of precipitates. This was calculated from the integrated intensity (as a proxy for the volume fraction) and the average radius (from which the volume of the average sized particle was calculated assuming a spherical morphology). The number density evolution calculated in this way (arbitrary units) is plotted as a function of strain and time in Fig. 4.e and 4.f respectively.

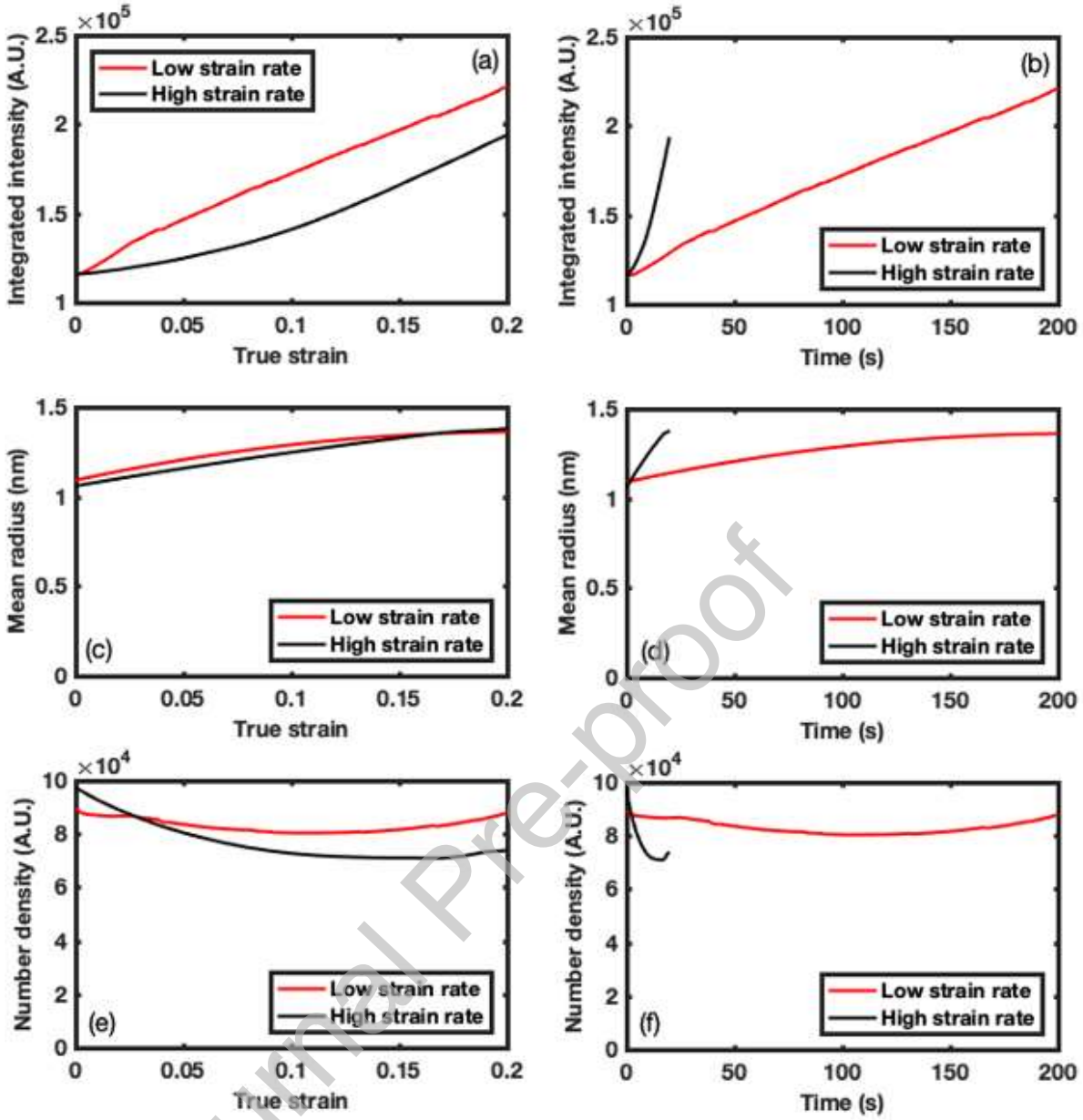

Fig. 4 Evolution of (a) integrated intensity versus true strain. (b) Integrated intensity versus time. (c) Mean radius versus true strain. (d) Mean radius versus time. (e) Number density versus true strain. (f) Number density versus time.

This shows that the number density did not increase during either the high or low strain rate tests. At the high strain rate, there is actually a slight decrease in the calculated number density during the test, and at the slow strain rate it remains almost constant. Although, there is likely to be significant error in this estimate due to the approximations inherent in the calculation, the results support the idea that the different behaviours observed at different strain rates is not due to differences in nucleation of new precipitates, but is controlled by growth and coarsening of precipitates formed during the pre-heating process. In the slow strain rate case, the integrated intensity increases more steeply as a function of strain

at low strain values compared with the high strain rate case. Since the radius evolution is similar in both cases, the cause of this difference is a small difference in the total number density evolution at low strains. The implication of the measurements is that in the high strain rate case, there is an initial reduction in the number density leading to a lower increase in the integrated intensity (with respect to strain) in the initial portion of the curve compared to the low strain rate case (Fig. 4(a)). These effects are small however, and the variation in number density is within the error expected for this parameter, so this apparent difference in behaviour may not be significant and it does not affect the subsequent analysis.

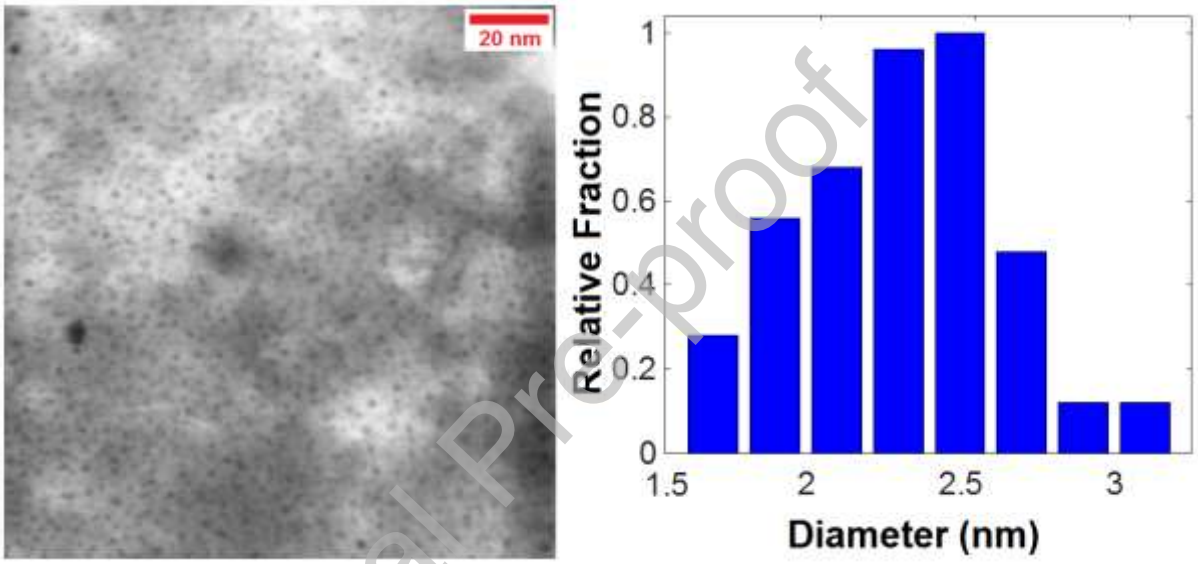

Fig. 5 Transmission electron micrograph of the slow strain sample with measured size distribution. Size distribution is represented as the relative fractions of each size group population compared to the mode diameter group (diameter range 2.4 - 2.6 nm).

The reliability of the SAXS data and post-acquisition analysis was assessed by comparing the SAXS measurements taken at the end of the deformation step with post-mortem TEM imaging. A representative TEM micrograph for the slow strain rate sample is shown in Fig. 5 with the measured size distribution. Deschamps and De Geuser [15] suggest a relationship for approximation of actual radius using the Guinier radius, 'Y$_{ث}$ (where, 'Y$_{ث}$ سي σ°⁷· ⁷ή . When this applies to our results, a reasonable agreement between the TEM imaging based average radius (1.21 nm) and the estimation from SAXS data (1.24 nm at the end of processing).

There was also no evidence of a bimodal precipitate population observed in the TEM, nor evidence that the deformation induced changes were a result of precipitation on

dislocations (the precipitates being homogeneous in their distribution in both the high and low strain rate specimens). This is consistent with previous observations, where precipitation on dislocations was not dominant in explaining dynamic interaction effects [7, 10].

4. Discussion

The experimental results presented here demonstrate the capability to conduct in-situ time resolved SAXS experiments with thicker specimens with relatively short time scales using high photon energy X-rays. In this initial experimental attempt, the selection of sample thickness/photon energy was not optimised. The selection of such parameters was predominantly based on technical constraints imposed by beamline instrumentation and the ETMT limitations. When considered with the sample sizes and time scales, the experiments demonstrate strong potential to reproduce and simulate the industrial forming process conditions. In particular, demonstrated work here overcomes some of the problems associated with SAXS experiments requiring deformation of sub-mm thick specimens, enabling to establish more representative stress-state levels encountered in actual processing. Small Angle Neutron Scattering (SANS) can also be used to study thicker specimens, but typical neutron fluxes are typically much weaker and cannot currently be used to conduct time resolved studies at the sampling speed available with SAXS to study metallic alloys.

4.1 Analysis of the strain rate dependence of dynamic precipitation

The results show that at both strain rates, simultaneous deformation and heating has led to an increase in the precipitate volume fraction and average particle radius that is consistent with growth and coarsening of an existing population formed during the natural ageing, pre-heat and holding steps. However, it should be noted that the hold and deformation temperature used in this study (190^{o}C, 463K) is relatively high for a precipitation heat treatment and results in rapid ageing [17].

As observed, the increase in average particle radius was very similar for specimens deformed at a strain rate of 10^{-3} and 10^{-2} s^{-1}, meaning that this change occurs 10 times faster at the higher strain rate. This result is in contrast to previous in-situ studies performed at lower strain rates and lower temperature (433 K) which found no correlation, within the large error inherent in the measurements, when growth rate was plotted as a function of strain rate [7].

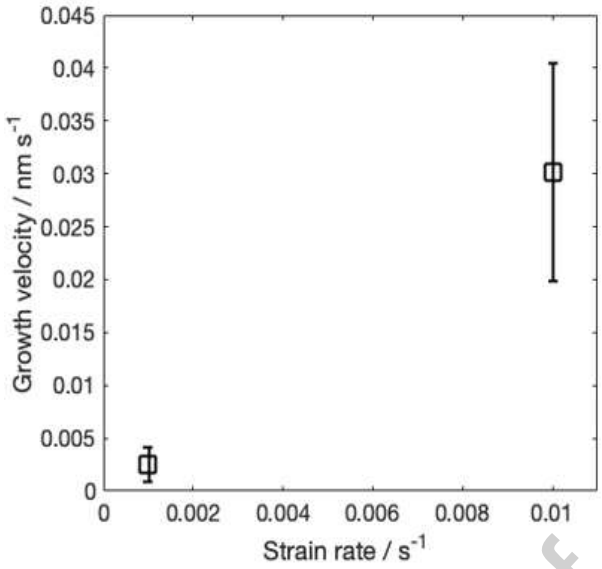

Fig. 6 The calculated growth velocity of the mean particle radius at both strain rates used in the present study (10^{-3} and 10^{-2} s^{-1}).

The growth velocity was determined by numerical differentiation of the mean radius data with respect to time and is plotted as a function of applied true strain in Fig. 6. This plot shows the large difference between the growth velocity (for a given strain) between the high and low strain rate conditions. It also shows a mean growth velocity that decreases with increasing true strain, which is opposite to the behaviour observed elsewhere, where the growth velocity increases with strain [7]. In the high strain rate case, there is an abrupt reduction in growth velocity when the applied true strain exceeds 0.17. It should be noted however that at the high strain rate the intervals in strain between measurements are quite large (0.01). A decreasing mean growth velocity with increasing strain is not expected if the only variable controlling growth velocity is solute diffusivity. However, the present case is more complicated than this, since the alloy also has supersaturated solute at the start of the experiment, and the degree of supersaturation also controls the growth rate (i.e. the pure coarsening regime is not established). The super-position of these effects could lead to a reducing growth velocity with strain, even if the solute diffusivity increased with strain. The reason for the apparently abrupt decrease in the growth velocity at high strain rate and high strain is unclear. It may correspond to an exhaustion of solute, or an establishment of a more stable precipitate distribution (the number density, which originial decreases, plateaus at higher strain as shown in Fig 4(e)). Deconvolution of these effects requires a different experiment (e.g. use of an initial condition where the solute is fully precipitated prior to deformation).

4.2 Excess Vacancy Model

As discussed in the introduction, previous studies have emphasised the dominant role played by deformation induced vacancies in accelerating precipitate evolution under dynamic conditions [7, 10, 11]. Other factors, such as direct precipitation on dislocations, or ballistic solute drag, are alone not sufficient to explain the accelerating effect of deformation on precipitation kinetics [6, 7, 9]. The vacancy model is also consistent with other observations, such as the uniformity of post-deformation precipitation [5, 10], and the observation that the accelerating effect of deformation is rapidly lost once deformation is stopped [7]. The present work was conducted in a regime of temperature and strain rate where deformation induced vacancy effects are likely to be dominant, and the observed post-deformed microstructures are also consistent with this mechanism. Therefore, consistent with the conclusions of previous authors [7-11] the results will be interpreted with the assumption that deformation induced vacancies provide the dominant accelerating effect in controlling the kinetics of precipitate evolution.

A commonly used simple model to predict the evolution of deformation induced vacancies originates from Militzer et al. [14]. This model is based on the premise that a strong enhancement in vacancy mediated diffusion occurs during plastic deformation due to excess vacancies δ_{ex} that are created because of non-conservative motion of jogs on screw dislocations. The production rate of excess vacancies can be written as;

$$\frac{d\delta_{ex}}{dt} = \frac{\alpha \sigma \dot{\varepsilon} \Omega}{E_f} \qquad (2)$$

Here, σ is the flow stress, Ω is the atomic volume, E_f is the vacancy formation energy, $\dot{\varepsilon}$ is the strain rate and α is constant representing the fraction of the applied work stored in the vacancies produced [18]. It should be noted that as equation 2 demonstrates, the production rate of excess vacancies is proportional to the strain rate.

These excess vacancies are not stable and will constantly seek to annihilate. In the model of Militzer et. al [14], annihilation is assumed to be controlled by diffusion of vacancies to sink sites. The sink sites considered in the model are grain boundaries and forest dislocations.

$$\frac{d\delta_{ex}}{dt} = D_v \delta_{ex} \left(\frac{\rho_f}{b} \right) \qquad (3)$$

Here, D_v is the diffusivity of vacancies, ρ_f is the forest dislocation density and Ω is the grain size. Since the grain size of the starting sample was several tens of microns (~100 μm), the contribution from the 2nd term of equation 3 is negligible in the present study. Upon combining equations 2 and 3 (ignoring the 2nd term), we obtain the evolution of excess vacancies during plastic deformation.

$$\frac{d\delta_v}{dt} = \frac{\dot{\varepsilon}_{eq} m}{b} D_v \rho_f \delta_v \qquad \tau$$

If the direct effect of deformation induced vacancies on the formation of new precipitate nuclei can be ignored (as is reasonable in the present case, since the precipitate number density did not increase) then the dominant effect of the extra vacancies will be to enhance solute diffusion rates [7, 10]. In the presence of excess vacancies, the effective diffusivity (D^{eff}) can be written as

$$D^{eff} = D \left(1 + \frac{\delta_v}{\delta_v^{eq}}\right) \qquad [5]$$

Where D and δ_v^{eq} are the thermal diffusivity and equilibrium vacancy concentration, respectively.

As equation 4 shows, the evolution behaviour of excess vacancies will depend on the balance between vacancy creation and vacancy annihilation. Furthermore, as equation 3 demonstrates, the annihilation rate is itself a function of the dislocation density and excess vacancy concentration and increases as the number of excess vacancies increase. For conditions where the annihilation term is small compared with the creation term, the excess vacancy concentration (found by integrating equation 2 with respect to time) will increase linearly with strain (ignoring any change in dislocation density) and will not be a function of strain rate [7]. However, as the vacancy concentration increases, so does the annihilation rate and eventually a steady state are reached where the creation and annihilation rates cancel. The value of the excess vacancy concentration when this steady-state is reached is a function of the strain rate, being greater when the strain rate is higher, but also the dislocation density, which will scale predominantly with strain at low temperatures.

The excess vacancy model is sensitive to a number of parameters whose values are poorly known for industrial aluminium alloys, such as that studied here. These parameters include the vacancy formation energy, vacancy diffusivity (which in turn is strongly dependent on the vacancy migration activation energy), dislocation arrangement, and proportion of the applied work that is stored. Relatively small changes to these parameters

can have a strong effect on the predictions. For example, the model can produce behaviours that are both strongly strain rate dependent, or strain rate independent, depending on the regime in which a particular experiment and combination of parameters produces.

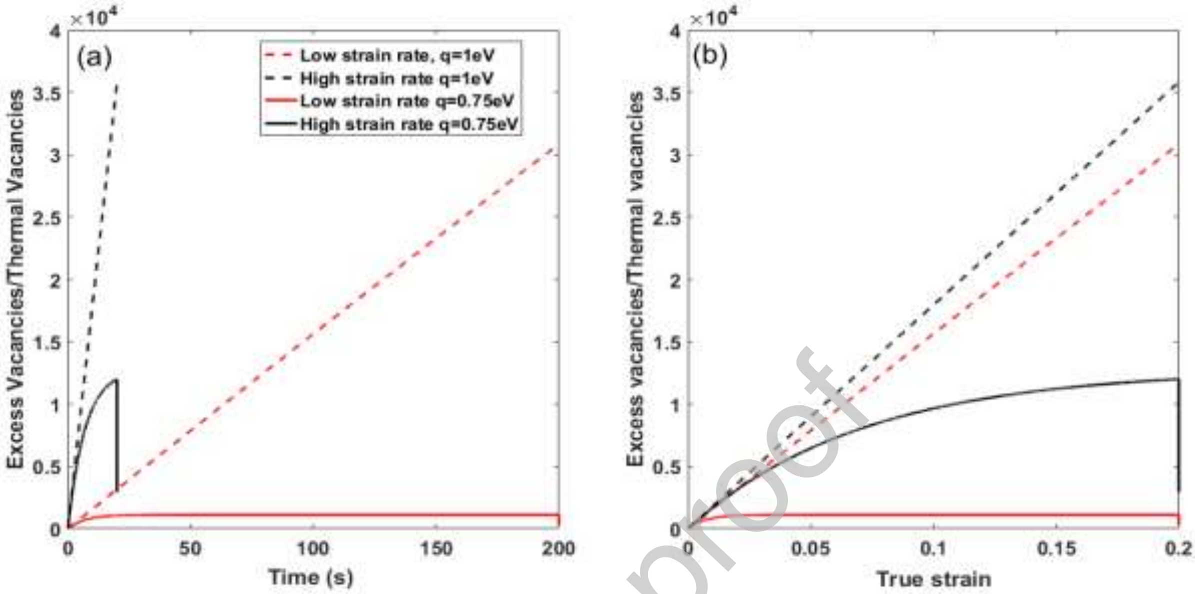

Fig. 7 Prediction of the excess vacancy fraction as (a) a function of time and (b) a function of true strain for both strain rates used in the present study (10^{-3} and 10^{-2} s^{-1}). Two estimates are used for the activation energy for vacancy migration (1 eV, upper bound and 0.75 eV, lower bound).

This is demonstrated in Fig.7, where the model has been applied to the conditions used in the present study. The input parameters have been taken directly from previous applications of this model to aluminium alloys [7] (ɱ سي ρ፟φφ% طي ςω Í ˈ ẖ Ǖ ي سي π፟χφ Å6ẖ … سي π፟ρ). One uncertain parameter is the activation energy for vacancy migration (Q_v) in 7xxx alloys. This has been taken as 1eV in previous work, which is an upper bound estimate [7]. The effect of reducing Q_v to 0.75 eV (a lower bound estimate) is also shown. In performing this calculation, the dislocation density has been assumed to be constant. Its value is also uncertain and practically difficult to measure during deformation since recovery occurs quickly in aluminium alloys.

As Fig. 7 shows, for the range of conditions used in this study, the excess vacancy evolution (which can be directly correlated to the precipitate growth rate [7]) can either show a near linear increase with little dependence on strain rate (for Q_v=1 eV) or can rapidly reach a plateau value, which is strongly strain rate dependent (for Q_v=0.75 eV), depending on the value chosen for the vacancy migration energy. Similar differences in behaviour can be

obtained by changing any other factor that alters the balance between vacancy creation and annihilation mechanisms (for example, an increase in dislocation density will also increase annihilation rate).

The present results, where the precipitate growth rate was measured to be a strong function of the strain rate for the same value of strain, therefore suggest the experiments were carried out in a regime where excess vacancy annihilation was significant and a steady state excess vacancy concentration was established rapidly during straining (as shown in Fig. 7 for a vacancy migration activation energy of 0.75 eV). Temperature is a critical factor in determining which regime is in operation. The deformation temperature used in the present work (463 K) was higher than that used in previous studies (e.g. 433 K in [7]). Since vacancy annihilation rate is very sensitive to temperature, even a small increase can lead to a transition from strain rate insensitive to strain rate sensitive (steady state) excess vacancy concentration regimes. This is likely to be a critical factor in explaining the difference between the sensitivities observed in this study and those in previous in-situ work.

5. Conclusions

A high photon energy synchrotron SAXS has been used to perform in-situ studies of dynamic precipitate evolution in a 7xxx aluminium alloy during deformation at a higher strain rates and on larger gauge volumes of material than previously reported. The experimental results have demonstrated the potential of using high photon energy X-rays to perform in-situ studies on dynamic precipitate evolution in metallic materials under conditions that closer to those experienced in the industrial forming processes.

The data obtained has revealed a strong acceleration in the evolution of precipitate size and volume fraction with an increase in strain rate from 10^{-3} to 10^{-2} s^{-1}. Over this range, the mean precipitate growth rate increased by approximately one order of magnitude. This more rapid growth rate was found to compensate for the order of magnitude decrease in time experienced by the material at the higher strain rate, meaning that the precipitate size as a function of strain was found to be nearly strain rate independent.

However, these new results contrast with previous in-situ work at lower strain rate, where the growth rate (rather than the size) of precipitates was found to proportional to strain but strain rate independent.

Both the present results and previous work be explained a model that assumes deformation induced vacancies have the dominant dynamic effect in accelerating the kinetics.

In previous work, vacancy annihilation was considered to be negligible, resulting in a different behaviour where there was only strain dependence. In the present work, our new results are reconciled by proposing that the excess vacancy concentration rapidly reaches a steady state value, which is expected to be strain rate dependent. This is likely to be due to the higher temperature used in the present study. It has been demonstrated that identifying which regime operates depends sensitively on the input parameters to the excess vacancy model, which are poorly defined. Further effort is therefore required to more accurately quantify these parameters if such a model is to be a useful tool in interpreting dynamic precipitation results.

Declaration of interests

☒ The authors declare that they have no known competing financial interests or personal relationships that could have appeared to influence the work reported in this paper.

Acknowledgements

The EPSRC are thanked for financial support through the associated programme grant LightFORM (EP/R001715/1) and EP/P02680X/1. Diamond Light Source (UK) is acknowledged for granting beam time to undertake the experiments at beamline I12 (EE13828). P.B. Prangnell is grateful to the Royal Academy of Engineering, UK, and Airbus for financial support through the Airbus-University of Manchester Centre for Metallurgical Excellence.

References

[1] W. Huo, L. Hou, Y. Zhang, J. Zhang, Warm formability and post-forming microstructure/property of high-strength AA 7075-T6 Al alloy, Materials Science and Engineering: A 675 (2016) 44-54.

[2] M. Kumar, C. Poletti, H.P. Degischer, Precipitation kinetics in warm forming of AW-7020 alloy, Materials Science and Engineering: A 561 (2013) 362-370.

[3] M. Kumar, N. Sotirov, C.M. Chimani, Investigations on warm forming of AW-7020-T6 alloy sheet, Journal of Materials Processing Technology 214(8) (2014) 1769-1776.

[4] M. Kumar, N.G. Ross, Influence of temper on the performance of a high-strength AlïZnï Mg alloy sheet in the warm forming processing chain, Journal of Materials Processing Technology 231 (2016) 189-198.

[5] K. Teichmann, C.D. Marioara, K.O. Pedersen, K. Marthinsen, The effect of simultaneous deformation and annealing on the precipitation behaviour and mechanical properties of an AlïMgïSi alloy, Materials Science and Engineering: A 565 (2013) 228-235.

[6] A. Deschamps, F. Bley, F. Livet, D. Fabregue, L. David, In-situ small-angle X-ray scattering study of dynamic precipitation in an Al-Zn-Mg-Cu alloy, Philosophical Magazine 83(6) (2003) 677-692.

[7] A. Deschamps, G. Fribourg, Y. Bréchet, J.L. Chemin, C.R. Hutchinson, In situ evaluation of dynamic precipitation during plastic straining of an AlïZnïMgïCu alloy, Acta Materialia 60(5) (2012) 1905-1916.

[8] J.D. Embury, A. Deschamps, Y. Brechet, The interaction of plasticity and diffusion controlled precipitation reactions, Scripta Materialia 49(10) (2003) 927-932.

[9] A. Deschamps, M. Niewczas, F. Bley, Y. Brechet, J.D. Embury, L.L. Sinq, F. Livet, J.P. Simon, Low-temperature dynamic precipitation in a supersaturated AI-Zn-Mg alloy and related strain hardening, Philosophical Magazine A 79(10) (1999) 2485-2504.

[10] C.R. Hutchinson, F. de Geuser, Y. Chen, A. Deschamps, Quantitative measurements of dynamic precipitation during fatigue of an AlïZnïMgï(Cu) alloy using small-angle X-ray scattering, Acta Materialia 74 (2014) 96-109.

[11] L. Couturier, A. Deschamps, F. De Geuser, F. Fazeli, W.J. Poole, An investigation of the strain dependence of dynamic precipitation in an Al-Zn-Mg-Cu alloy, Scripta Materialia 136 (2017) 120-123.

[12] C.R. Hutchinson, P.T. Loo, T.J. Bastow, A.J. Hill, J. da Costa Teixeira, Quantifying the strain-induced dissolution of precipitates in Al alloy microstructures using nuclear magnetic resonance, Acta Materialia 57(19) (2009) 5645-5653.

[13] Y. Chen, M. Weyland, C.R. Hutchinson, The effect of interrupted aging on the yield strength and uniform elongation of precipitation-hardened Al alloys, Acta Materialia 61(15) (2013) 5877-5894.

[14] M. Militzer, W.P. Sun, J.J. Jonas, Modelling the effect of deformation-induced vacancies on segregation and precipitation, Acta Metallurgica et Materialia 42(1) (1994) 133-141.

[15] A. Deschamps, F. De Geuser, On the validity of simple precipitate size measurements by small-angle scattering in metallic systems, Journal of Applied Crystallography 44(2) (2011) 343-352.

[16] A. Deschamps, F. de Geuser, Quantitative Characterization of Precipitate Microstructures in Metallic Alloys Using Small-Angle Scattering, Metallurgical and Materials Transactions A 44(1) (2013) 77-86.

[17] R. Nolan, Microstructure Formability Relationships in New Generation High Strength Aluminium Automotive Alloys, DAI-C 75/01, Dissertation Abstracts International (2015).

[18] H. Mecking, Y. Estrin, The effect of vacancy generation on plastic deformation, Scripta Metallurgica 14(7) (1980) 815-819.

Graphical abstract